Letter

Non-Hermitian topological exciton-polariton corner modes

Xingran Xu [1,2,*,†] Ruiqi Bao [2,*] and Timothy C. H. Liew [2,‡]
[1]*School of Science, Jiangnan University, Wuxi 214122, China*
[2]*Division of Physics and Applied Physics, School of Physical and Mathematical Sciences, Nanyang Technological University, Singapore 637371, Singapore*

(Received 14 February 2022; revised 24 October 2022; accepted 25 October 2022; published 7 November 2022; corrected 13 April 2023)

Non-Hermitian topological corner modes can be formed in exciton-polariton lattices under nonresonant pumping. Signals propagating in the bulk of the system can travel around defects, which is not possible in one-dimensional topological lattices or two-dimensional lattices with Hermitian edge states. In the presence of nonlinear interactions, the system remains topological, as evidenced by the winding of the complex fluctuation spectrum. Finally, as *all* polariton states are localized, the system offers an opportunity for more accurate measurement of the polariton-polariton interaction strength as one can avoid condensing in a state with large overlap with the pump-induced exciton-reservoir.

DOI: 10.1103/PhysRevB.106.L201302

Introduction. Exciton-polaritons are part-light part-matter quasiparticles formed in semiconductor microcavities [1–4]. Their matter component offers significant nonlinearity, while their optical component allows manipulation [5] and observation on optical lengthscales. With their pseudospin [6], this offers a unique system to study spinor wave behavior in a controllable and accessible environment. One of the most famous physical phenomena in this system is known as *polariton superfluidity*, which is traditionally characterized by the propagation of a polariton wave packet around a defect without coupling to backscattered states [7]. After its prediction [8] it was generalized to the spinor case [9] and later observed experimentally [10], up to room temperature in modern materials [11].

The absence of coupling to backscattered states is not a unique effect of nonlinearity. Topological Chern systems are also famous for the same claim and well established in topological photonics as well as in polaritonic crystals formed by the etching of semiconductor microcavity lattices [12]. The difference though in the observable behavior (aside the underlying physical mechanism) is that the backscattering suppression for a polariton superfluid should occur for a wave packet propagating in the bulk of the system, while the suppression in a Chern insulator occurs for a wave packet propagating along the edge of a lattice. The first situation seems more favorable for application in coherent polariton devices [13].

While topological Chern systems are an example of Hermitian physics, it should be noted that polaritons are non-Hermitian systems [14,15]. Non-Hermitian systems can possess unique properties. During the past two decades, parity-time (PT) symmetry has attracted a lot of research interest [16–18]. In contrast to the view that only Hermitian Hamiltonians have real eigenvalues, non-Hermitian Hamiltonians that commute with the parity-time operator can also have real spectra. In the polariton system, the application of a nonresonant optical field, which can be spatially patterned or modulated, represents a gain in the system, while the finite lifetime of polaritons represents a natural loss. The gain-loss control of polaritons makes it a great platform to study non-Hermitian physics and energy spectra may be complex.

Non-Hermitian lattices allow non-Hermitian topological effects, such as the skin effect [19–23] where *all* the eigenstates of a system become localized at an edge and a new bulk-boundary correspondence requires a generalized Brillouin zone (GBZ) method for its explanation [24–27]. The simplest one-dimensional (1D) skin effect can be realized in the Hatano-Nelson (HN) model [28,29], which assumes a nonreciprocal hopping between lattice sites. The Chern number is replaced with a different topological invariant, namely, a winding number describing the angular direction in which eigenenergies encircle a point in the complex plane when the wave vector is scanned across the Brillouin zone. If the skin effect is present, then the eigenenergies calculated for an infinite lattice with periodic beriodic boundary condition (PBC) should also encircle the eigenenergies calculated for a finite lattice with otherwise the same parameters and open boundary condition (OBC) [21,26,30]. To realize the skin effect, coupled resonant optical waveguides [31–33] are typically considered for coupling ring resonators in a lattice [34–38]. In exciton-polariton systems, the skin effect was predicted in a one-dimensional lattice [38,39] using a circularly polarized gain [40] to break spin symmetry and induce an effective asymmetric coupling between sites.

Here, we design a two-dimensional (2D) polariton lattice, where all eigenstates are localized at its corners. Wave packets propagating in the bulk of the system are found to travel around defects, in analogy to polariton superfluids although there is coupling to other forward propagating states and the

*These authors contributed equally as the first author to this work.
†thoexxr@hotmail.com
‡TimothyLiew@ntu.edu.sg

underlying physical mechanism is very different: The skin effect does not require particle-particle interactions for its realization. In such a regime, the spectral winding number of the linear Hamiltonian constitutes an effective topological invariant.

Even though particle-particle interactions are not required for the skin effect, it is instructive to ask whether they would affect the topology. This is not a straightforward question: Topological invariants are defined from the eigenstates of linear Hamiltonians, which no longer exist in the nonlinear regime. To address this, we first point out that driven-dissipative systems often form in a dominant state (of highest gain) or stationary state (if there is gain saturation). However, if only a single such state appears, it is not enough to determine the system topology: We need other states to exist. These can only be the states of fluctuations on top of the dominant or stationary state and we indeed show that a non-trivial fluctuation spectral winding exists. As this spectrum exists in the presence of interactions, we can still identify nonlinear driven-dissipative systems as topological.

Finally, we note that a critical challenge in the field has been the measurement of the polariton-polariton interaction strength. This is inferred from the energy shift of interacting polaritons, however, this is also affected by interactions of polaritons with a reservoir of higher-energy states. Unfortunately, as polaritons typically form in the state with maximum overlap with this reservoir, that is, the state of highest gain, the unwanted interaction is heavily maximized. This resulted in spurious measurements spanning orders of magnitude [41]. An exceptional case is in ultra-high-quality factor microcavities, where polaritons live long enough to transition from states with maximum overlap with the reservoir to those that have small overlap [41,42]. However, this is not possible in most microcavities, especially those in novel materials [43,44]. In the case of the skin effect though, as all states are localized at the corners, one can avoid condensing in a state that has high overlap with the exciton reservoir to begin with.

We consider first a tight-binding model of a spinor square lattice with onsite gain

$$i\hbar\frac{\partial\psi_{m,n,\pm}}{\partial t} = Ae^{\pm 2i\pi(m+n)/N}\psi_{m,n,\mp} - i\Gamma_{\pm}\psi_{m,n,\pm} + J(\psi_{m-1,n,\pm} + \psi_{m+1,n,\pm} + \psi_{m,n-1,\pm} + \psi_{m,n+1,\pm}). \quad (1)$$

Here m and n are site indices. $\pm$ denotes an on-site spin degree of freedom, where different spins have different decay rates $\Gamma_{\pm}$. J is the intersite coupling strength, and A is a coupling strength between spins, where the phase of the coupling is site dependent with N the number of sites in each direction of the unit cell. Such a lattice could be realized with exciton-polaritons in microcavities. The coupling between spins is equivalent to a local polarization splitting, which could be arranged using elliptical micropillars [40,45]. The orientation of the pillars [illustrated by the grey ellipses in Fig. 1(b)] define a site-dependent phase of the coupling between spin components. The different gain for different spin components could be achieved with an elliptically polarized nonresonant pumping. We begin by considering linear physics, but will later consider the effect of interactions as well as gain saturation.

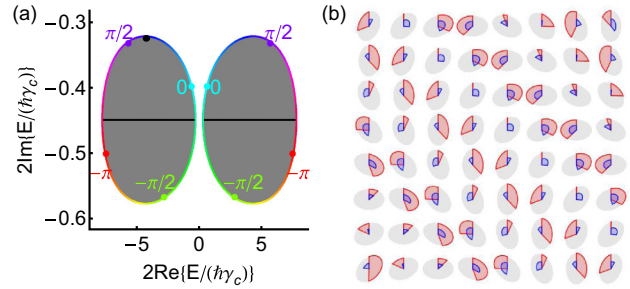

FIG. 1. (a) Complex energy spectrum of Eq. (1) for open (black) and periodic (grey) boundaries. The colored loops show the energies for periodic boundaries for a diagonal contour across the Brillouin zone with the values of the wave vector marked. (b) The state corresponding to maximum gain marked by the black dot in (a). The light gray ellipses mark the orientation of micropillars used to realize local polarization splitting. The radial size of elliptical arcs shows the amplitude of + (red) and − (blue) spin components. The arc lengths are proportional to their corresponding phases, with a complete revolution corresponding to 2π. Parameters: $J = \hbar\gamma_C/2$, $A = 2\hbar\gamma_C$, $\Gamma_+ = 0.05\hbar\gamma_C$, $\Gamma_- = 0.4\hbar\gamma_C$, $N = 8$. γ_C sets the inverse timescale of the system, corresponding to the decay rate in polariton systems.

Non-Hermitian corner modes. The eigenstates of Eq. (1) have a complex energy spectrum shown in Fig. 1(a) for a finite lattice with OBC (black) and an infinite lattice with PBC (grey). Along a diagonal contour in the reciprocal space corresponding to m and n directions the eigenenergies with periodic boundaries form the loops illustrated with colors. These loops define complex spectral winding numbers [26,46,47], ± 1, which represent a nontrivial topology in the system. The OBC energies are encircled by the PBC in the complex plane, which is a key characteristic of the non-Hermitian skin effect [30,48–51]. Figure 1(b) shows the state of highest gain in the system with PBC. Note that the phase gradient is along the diagonal direction; indeed it is because states on the edge of the shaded region in Fig. 1(a) correspond to states with diagonal wave vectors that a contour along such wave vectors in the Brillouin zone is the best for defining the winding number [52].

Furthermore, all positive energy states are localized at the top-right corner of a finite lattice, while all negative energy states are localized at the bottom-left corner [53–55], as shown in Fig. 2. In contrast to the corner states of Hermitian systems [56–59], we stress that it is all the states of the considered non-Hermitian system, not just a selection, that are localized at corners. Although throughout the main text we base our results on a tight-binding model (where the elliptical shape of the pillars manifests in a polarization splitting with specific alignment), we consider a continuous model that accounts explicitly for the spatial shape of the elliptical pillars and find similar results [60].

Signal propagation. The skin effect gives all wave functions a nonreciprocal flux toward a boundary. In one-dimensional lattices showing the skin effect (e.g., in the HN model) this may enhance propagation in one direction while weakening propagation in the other. However, if there is a defect in the lattice, the signal has a low chance to cross the defect and most of the propagation will stop at the defect (aside

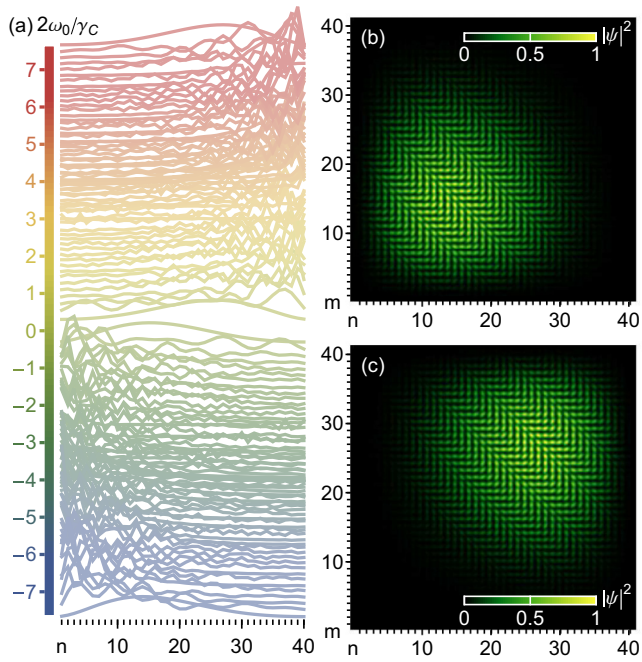

FIG. 2. (a) Intensity distribution of selected eigenstates with different energies along the n-direction (the distribution is the same along the m-direction due to symmetry). (b), (c) show the spatial distributions of the lowest- and highest-energy states, respectively. The 40×40 sites used in this calculation are obtained by repeating the unit cell in Fig. 1 five times in each direction. Parameters are the same as in Fig. 1. Although attained with a tight-binding model, the intensity of each site is drawn as an elliptical Gaussian to illustrate the orientations of micropillars in an exciton-polariton realization.

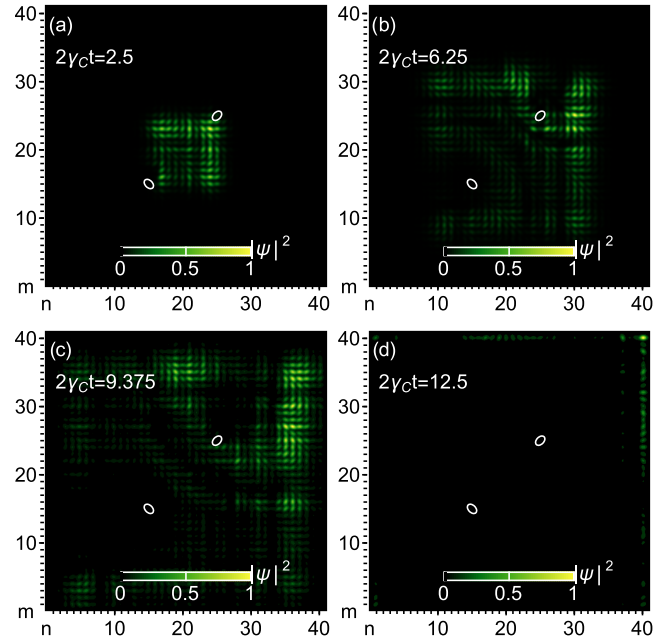

FIG. 3. Time evolution of an initial wave packet with two defects at $(n, m) = (15, 15)$ and (25,25) sites (white ellipses). Parameters are the same as in Fig. 1. The defect sites have an added potential energy of $6\hbar\gamma_C$. In all panels the intensity is normalized to the maximum value. In practice, the overall intensity changes in time according to the imaginary components of the eigenvalues calculated in Fig. 1(a). For our parameters, the imaginary components are negative, corresponding a decay. In principle, by increasing the pumping strength the decay can be slowed or even turned into growth.

from a small amount allowed by quantum tunneling). The higher-dimensional non-Hermitian corner modes give more flexibility for the signal to propagate efficiently and allow direction to be controlled. Defects can be circumvented and do not stop propagation, as shown in Fig. 3.

Here an initial wave packet localized at the center of the lattice initially appears to spread out in all directions [Fig. 3(a)]. At intermediate times, the wave packets appear to propagate around the defects [Figs. 3(b) and 3(c)], while some intensity from slower moving components of the wave packets remains in between the two defects. At longer times, we see clearly that the entire wave packet moved to the top-right corner [Fig. 3(d)] showing the directional behavior of the propagation in this system. There is no intensity in the lower left-half of the lattice, implying no backscattered component.

We also considered a system with a line defect as shown by the white dashed line in Fig. 4. The line defect divides the system into two parts: The left part has potential $V = -0.1\hbar\gamma_C$; the right part has potential $V = 0.1\hbar\gamma_C$. Here the energy difference we choose is less than the energy gap. We can still see polaritons passing the line defect, which shows that our proposed system has robustness to the line defect.

Topology in the nonlinear regime. In systems with a Kerr nonlinearity, such as exciton-polaritons, Eq. (1) should be supplemented with a term $g|\psi_{n,m,\pm}|^2\psi_{n,m,\pm}$ in the right-hand side, with g the interaction strength. In this case the winding number can no longer be defined as we have no

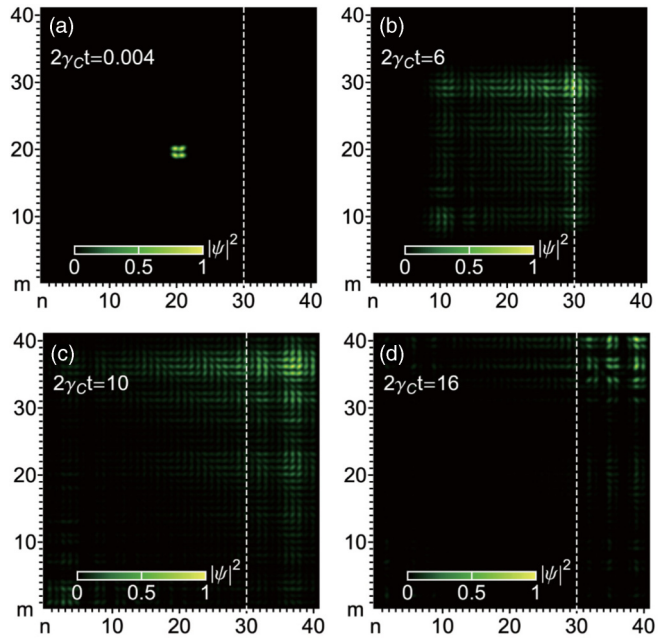

FIG. 4. Time evolution of the 2D polaritons with a line defect, which is along the y direction as shown by the white dashed line (a)–(d). Parameters are taken the same as in Fig. 1 with the added line defect potential.

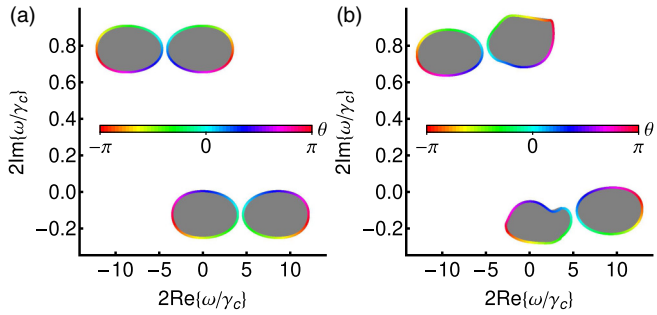

FIG. 5. Fluctuation spectrum of Eq. (1) constructed on top of the highest gain state with (a) $g = 0$ and (b) $g = 25\hbar\gamma_C$.

eigenstates. However, it can also be noted that the system can be expected to form dominantly in a state of highest gain [Fig. 1(b)]. In the presence of such a highly occupied state, the spectrum of the system is rather defined by the Bogoliubov–de Gennes fluctuation spectrum obtained by substituting $\psi_{n,m,\pm} = e^{-i\omega_0 t}(\psi^{(0)}_{m,n,\pm} + u_{m,n,\pm}e^{-i\omega t} + v^*_{m,n,\pm}e^{i\omega^* t})$, where $\psi^{(0)}_{m,n,\pm}$ is the dominant (possibly growing) state of the system with (complex) energy ω_0; $u_{m,n,\pm}$ and $v^*_{m,n,\pm}$ are the amplitudes of small fluctuations with frequency ω and $-\omega^*$, respectively. Substitution into Eq. (1) and keeping linear terms in $u_{m,n,\pm}$ and $v^*_{m,n,\pm}$ defines an eigenvalue problem for attaining the energies of fluctuations [61]. These are shown in the absence and presence of interactions in Fig. 5. We note that the spectral winding is present in the fluctuation spectrum of the driven-dissipative and propose that it is an equally valid measure of topology as the eigenstates of the linear Hamiltonian. The fluctuation spectral winding persists in the presence of interactions, confirming that the system is still topological. We note that Hermitian topology was predicted for fluctuation spectra in different geometries, but as far as we know non-Hermitian topology such as the one that we study here was not considered [62,63].

For larger nonlinearity, the distribution of the eigenvalues in the complex plane becomes more and more distorted, beyond that shown in Fig. 5(b). Eventually, the eigenvalues become so distorted that we were unable to define their winding number. This might be a limitation though of the algorithm that we use to define the winding number or a limitation of the contour that we choose in the reciprocal space. Whether the topology can be destroyed for very strong nonlinearity remains an open question.

Gain saturation. So far we considered a simplified model with constant gain represented by $\Gamma_\pm$. While this model may be accurate at early times, at long times the positive gain in this model will cause the intensity to grow unphysically to infinity. Of course this does not happen in real systems as the gain should be supplemented by saturation. Typically, this is handled in exciton-polariton systems by the replacement in Eq. (1)

$$i\Gamma_\pm \to \frac{i\hbar}{2}(RN_{m,n,\pm} - \gamma_C), \tag{2}$$

where R defines the rate of scattering of excitons from a reservoir with on-site population $N_{m,n,\pm}$ and γ_C is the polariton decay rate. The exciton reservoir evolves as

$$\frac{\partial N_{n,m,\pm}}{\partial t} = P_\pm - (\gamma_R + R|\psi_{n,m,\pm}|^2)N_{m,n,\pm}, \tag{3}$$

where $P_\pm$ is the intensity of the circularly polarized components of a nonresonant optical field and γ_R is the reservoir decay rate. This is not trivial, as the formation of a stationary state implies a balance of gain and loss, which might be interpreted as removing the non-Hermiticity of the effective Hamiltonian. However, we find that it is the nonlinear terms themselves that preserve the complex winding of the spectrum.

Interaction measurement. Despite its importance as a key parameter in polariton physics, the strength of polariton-polariton interaction is not easy to distinguish experimentally. One typically hopes to infer it from a nonlinear shift of the polariton energies, however, a severe complication is that the shift in energy of a polariton condensate can be associated to two terms:

$$V_c = \frac{\sum_{m,n,\pm} g|\psi_{m,n,\pm}|^4}{\sum_{m,n,\pm}|\psi_{m,n,\pm}|^2}, \tag{4}$$

and

$$V_r = \frac{\sum_{m,n,\pm}(g_R N_{m,n,\pm} + GP_{m,n,\pm})|\psi_{m,n,\pm}|^2}{\sum_{m,n,\pm}|\psi_{m,n,\pm}|^2}. \tag{5}$$

The first represents the interaction strength due to polariton-polariton interaction, while the second represents the interaction strength due to polariton-reservoir interaction. The reservoir-induced energy shift contains both a shift due to the modeled reservoir density, where g_R is the the reservoir-polariton interaction constant [64] and a term proportional to the on-site pumping $P_{m,n,\pm}$, which accounts for other hot carriers excited by the pumping [65]. In an experiment, the total measured blueshift is typically measured with increasing pumping strength, where it can be taken as the shift of the polariton condensate spectral line from the case at threshold. That is, if V_c^0 and V_r^0 denote the above quantities at threshold, then the measured blueshift is the sum of $\Delta V_c = V_c - V_c^0$ and $\Delta V_r = V_r - V_r^0$. Ideally, one hopes that ΔV_r is small, so that what is measured can be assumed to be ΔV_c and from this g can be extracted from a separate estimate of polariton densities. In practice though, ΔV_r is not negligible in typical geometries since the condensate typically forms in a state where there is maximum overlap with the exciton reservoir.

To account for the aforementioned interactions in our case, we include a term $g_R N_{m,n,\pm} + GP_{m,n,\pm}$ in the right-hand side of Eq. (1). We consider the case of a spatially uniform pumping at the condensation threshold, superimposed with an additional pumping spot in the center of the lattice that takes us beyond threshold.

For the 2D skin lattice, ΔV_r is around 20% of ΔV_c just above threshold. It is not zero, as there is still a finite overlap of the corner state with the reservoir, however, it is about three times smaller than the size of the reservoir-induced blueshift in the corresponding regular lattice, such that it is a much better approximation to neglect the reservoir-induced shift in the case of the skin lattice. In principle, a similar effect could be expected in 1D lattices, however, there is less delocalization

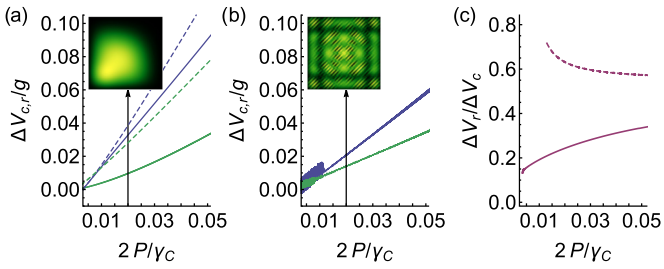

FIG. 6. Contributions to energy blueshift from threshold ΔV_c (blue) and ΔV_r (green) for 2D skin effect lattice [(a), solid, $N = 8$], corresponding 1D lattice [(a), dashed], and regular 2D lattice [(b), $N = 1$]. The insets show the intensity patterns in a 40×40 lattice at the indicated intensities. (c) Ratio $\Delta V_r/\Delta V_c$ for $N = 8$ (solid) and $N = 1$ (dashed) 2D lattice. Here polaritons are localized at the bottom-left corner which is due to $P_+ < P_-$. Parameters: $\gamma_R = 4\gamma_C/2$, $R = \gamma_C/2$, $g = 0.06\hbar\gamma_C$, $g_R = 2g$, $G = 0.0175$ (these are consistent with [64,65]). The pumping was taken with a uniform background of $P_+ = 1.996\gamma_C/2$ and $P_- = 5.996\gamma_C/2$ with an additional Gaussian spot (width ten sites) of varying intensity P exciting both spin components. Other parameters were the same as in Fig. 1.

between the edge state and reservoir in this case, resulting in the dashed lines in Fig. 6(a).

Compared to Figs. 6(a) and 6(b) shows the reservoir-induced blueshift ΔV_r (green) and the polariton-polariton interaction-induced blueshift ΔV_c (blue) for increasing pumping powers. The corresponding ratio of these two quantities is around 60% (or even higher for smaller pump powers) and compared to the ratio for the 2D skin effect lattice in Fig. 6(c). In other words, our scheme of topological non-Hermitian corner states reduces the effect of the reservoir on the blueshift by about three times.

Conclusion. we introduced a scheme for a 2D non-Hermitian skin effect in an exciton-polariton lattice. The combination of different gain rates of different spin components and a position-dependent phase hopping leads to non-Hermitian corner modes. As such a system is expected to form in the state of highest gain, its spectrum should be defined by that of fluctuations about this state. Topological invariants in the form of spectral winding numbers can be defined within this fluctuation spectrum. As the fluctuation spectrum still exists in the nonlinear regime, we are able to ascertain that the system remains topological in the presence of nonlinear interactions.

We give two applications of the higher-dimensional non-Hermitian topology. First, propagating polariton wavepackets *in the bulk* travel around defects. Second, as in the skin effect *all* the modes of the system can be localized and we can avoid the existence of any mode with high overlap with the exciton-reservoir, the system offers an opportunity to more accurately access the polariton interaction strength in systems with limited lifetime.

Acknowledgments. We thank Huawen Xu for stimulated discussing. This work was supported by the Singaporean Ministry of Education, via the Tier 2 Academic Research Fund Project No. MOE2019-T2-1-004.

[1] H. Deng, H. Haug, and Y. Yamamoto, Exciton-polariton Bose-Einstein condensation, Rev. Mod. Phys. **82**, 1489 (2010).
[2] J. Keeling and N. G. Berloff, Exciton-polariton condensation, Contemp. Phys. **52**, 131 (2011).
[3] T. Byrnes, N. Y. Kim, and Y. Yamamoto, Exciton-polariton condensates, Nat. Phys. **10**, 803 (2014).
[4] I. Carusotto and C. Ciuti, Quantum fluids of light, Rev. Mod. Phys. **85**, 299 (2013).
[5] C. Schneider, K. Winkler, M. D. Fraser, M. Kamp, Y. Yamamoto, E. A. Ostrovskaya, and S. Höfling, *Exciton-Polariton Trapping and Potential Landscape Engineering* (IOP, Washington, D.C., 2016), Vol. 80, p. 016503.
[6] I. A. Shelykh, A. V. Kavokin, Y. G. Rubo, T. C. H. Liew, and G. Malpuech, Polariton polarization-sensitive phenomena in planar semiconductor microcavities, Semicond. Sci. Technol. **25**, 013001 (2010).
[7] D. D. Solnyshkov, C. Leblanc, L. Bessonart, A. Nalitov, J. Ren, Q. Liao, F. Li, and G. Malpuech, Quantum metric and wave packets at exceptional points in non-Hermitian systems, Phys. Rev. B **103**, 125302 (2021).
[8] I. Carusotto and C. Ciuti, Probing Microcavity Polariton Superfluidity through Resonant Rayleigh Scattering, Phys. Rev. Lett. **93**, 166401 (2004).
[9] I. A. Shelykh, Y. G. Rubo, G. Malpuech, D. D. Solnyshkov, and A. Kavokin, Polarization and Propagation of Polariton Condensates, Phys. Rev. Lett. **97**, 066402 (2006).
[10] A. Amo, J. Lefrère, S. Pigeon, C. Adrados, C. Ciuti, I. Carusotto, R. Houdré, E. Giacobino, and A. Bramati, Superfluidity of polaritons in semiconductor microcavities, Nat. Phys. **5**, 805 (2009).
[11] G. Lerario, A. Fieramosca, F. Barachati, D. Ballarini, K. S. Daskalakis, L. Dominici, M. D. Giorgi, S. A. Maier, G. Gigli, S. Kéna-Cohen, and D. Sanvitto, Room-temperature superfluidity in a polariton condensate, Nat. Phys. **13**, 837 (2017).
[12] S. Klembt, T. H. Harder, O. A. Egorov, K. Winkler, R. Ge, M. A. Bandres, M. Emmerling, L. Worschech, T. C. H. Liew, M. Segev, C. Schneider, and S. Höfling, Exciton-polariton topological insulator, Nature (London) **562**, 552 (2018).
[13] M. D. Fraser, Coherent exciton-polariton devices, Semicond. Sci. Technol. **32**, 093003 (2017).
[14] T. Gao, E. Estrecho, K. Y. Bliokh, T. C. H. Liew, M. D. Fraser, S. Brodbeck, M. Kamp, C. Schneider, S. Höfling, Y. Yamamoto, F. Nori, Y. S. Kivshar, A. G. Truscott, R. G. Dall, and E. A. Ostrovskaya, Observation of non-Hermitian degeneracies in a chaotic exciton-polariton billiard, Nature (London) **526**, 554 (2015).
[15] R. Hanai, A. Edelman, Y. Ohashi, and P. B. Littlewood, Non-Hermitian Phase Transition from a Polariton Bose-Einstein Condensate to a Photon Laser, Phys. Rev. Lett. **122**, 185301 (2019).
[16] L. Feng, R. El-Ganainy, and L. Ge, Non-Hermitian photonics based on parity–time symmetry, Nat. Photonics **11**, 752 (2017).

[17] C. M. Bender and S. Boettcher, Real Spectra in Non-Hermitian Hamiltonians having PT Symmetry, Phys. Rev. Lett. **80**, 5243 (1998).

[18] R. El-Ganainy, K. G. Makris, M. Khajavikhan, Z. H. Musslimani, S. Rotter, and D. N. Christodoulides, Non-Hermitian physics and PT symmetry, Nat. Phys. **14**, 11 (2018).

[19] T. Helbig, T. Hofmann, S. Imhof, M. Abdelghany, T. Kiessling, L. W. Molenkamp, C. H. Lee, A. Szameit, M. Greiter, and R. Thomale, Generalized bulk–boundary correspondence in non-Hermitian topolectrical circuits, Nat. Phys. **16**, 747 (2020).

[20] L. Xiao, T. Deng, K. Wang, G. Zhu, Z. Wang, W. Yi, and P. Xue, Non-Hermitian bulk–boundary correspondence in quantum dynamics, Nat. Phys. **16**, 761 (2020).

[21] L. Li, C. H. Lee, S. Mu, and J. Gong, Critical non-Hermitian skin effect, Nat. Commun. **11**, 5491 (2020).

[22] C.-H. Liu, K. Zhang, Z. Yang, and S. Chen, Helical damping and dynamical critical skin effect in open quantum systems, Phys. Rev. Res. **2**, 043167 (2020).

[23] C. H. Lee, L. Li, and J. Gong, Hybrid Higher-Order Skin-Topological Modes in Nonreciprocal Systems, Phys. Rev. Lett. **123**, 016805 (2019).

[24] K. Yokomizo and S. Murakami, Non-Bloch Band Theory of Non-Hermitian Systems, Phys. Rev. Lett. **123**, 066404 (2019).

[25] D. S. Borgnia, A. J. Kruchkov, and R.-J. Slager, Non-Hermitian Boundary Modes and Topology, Phys. Rev. Lett. **124**, 056802 (2020).

[26] N. Okuma, K. Kawabata, K. Shiozaki, and M. Sato, Topological Origin of Non-Hermitian Skin Effects, Phys. Rev. Lett. **124**, 086801 (2020).

[27] S. Yao and Z. Wang, Edge States and Topological Invariants of Non-Hermitian Systems, Phys. Rev. Lett. **121**, 086803 (2018).

[28] N. Hatano and D. R. Nelson, Localization Transitions in Non-Hermitian Quantum Mechanics, Phys. Rev. Lett. **77**, 570 (1996).

[29] N. Hatano and D. R. Nelson, Vortex pinning and non-Hermitian quantum mechanics, Phys. Rev. B **56**, 8651 (1997).

[30] K. Zhang, Z. Yang, and C. Fang, Universal non-Hermitian skin effect in two and higher dimensions, Nat. Commun. **13**, 2496 (2022).

[31] Z. J. Wong, Y.-L. Xu, J. Kim, K. O'Brien, Y. Wang, L. Feng, and X. Zhang, Lasing and anti-lasing in a single cavity, Nat. Photonics **10**, 796 (2016).

[32] M. Hafezi, S. Mittal, J. Fan, A. Migdall, and J. M. Taylor, Imaging topological edge states in silicon photonics, Nat. Photonics **7**, 1001 (2013).

[33] B. Bahari, A. Ndao, F. Vallini, A. E. Amili, Y. Fainman, and B. Kanté, Nonreciprocal lasing in topological cavities of arbitrary geometries, Science **358**, 636 (2017).

[34] Z. Lin, L. Ding, S. Ke, and X. Li, Steering non-Hermitian skin modes by synthetic gauge fields in optical ring resonators, Opt. Lett. **46**, 3512 (2021).

[35] X. Zhu, H. Wang, S. K. Gupta, H. Zhang, B. Xie, M. Lu, and Y. Chen, Photonic non-Hermitian skin effect and non-Bloch bulk-boundary correspondence, Phys. Rev. Res. **2**, 013280 (2020).

[36] M. Y. Nada, M. A. K. Othman, and F. Capolino, Theory of coupled resonator optical waveguides exhibiting high-order exceptional points of degeneracy, Phys. Rev. B **96**, 184304 (2017).

[37] H. Xu, K. Dini, X. Xu, R. Banerjee, S. Mandal, and T. C. H. Liew, Nonreciprocal exciton-polariton ring lattices, Phys. Rev. B **104**, 195301 (2021).

[38] S. Mandal, R. Banerjee, E. A. Ostrovskaya, and T. C. H. Liew, Nonreciprocal Transport of Exciton Polaritons in a Non-Hermitian Chain, Phys. Rev. Lett. **125**, 123902 (2020).

[39] S. Mandal, R. Banerjee, and T. C. H. Liew, From the topological spin-Hall effect to the non-Hermitian skin effect in an elliptical micropillar chain, ACS Photonics **9**, 527 (2022).

[40] M. Klaas, O. A. Egorov, T. C. H. Liew, A. Nalitov, V. Marković, H. Suchomel, T. H. Harder, S. Betzold, E. A. Ostrovskaya, A. Kavokin, S. Klembt, S. Höfling, and C. Schneider, Nonresonant spin selection methods and polarization control in exciton-polariton condensates, Phys. Rev. B **99**, 115303 (2019).

[41] E. Estrecho, T. Gao, N. Bobrovska, D. Comber-Todd, M. D. Fraser, M. Steger, K. West, L. N. Pfeiffer, J. Levinsen, M. M. Parish, T. C. H. Liew, M. Matuszewski, D. W. Snoke, A. G. Truscott, and E. A. Ostrovskaya, Direct measurement of polariton-polariton interaction strength in the Thomas-Fermi regime of exciton-polariton condensation, Phys. Rev. B **100**, 035306 (2019).

[42] Y. Sun, Y. Yoon, M. Steger, G. Liu, L. N. Pfeiffer, K. West, D. W. Snoke, and K. A. Nelson, Direct measurement of polariton–polariton interaction strength, Nat. Phys. **13**, 870 (2017).

[43] C. Anton-Solanas, M. Waldherr, M. Klaas, H. Suchomel, T. H. Harder, H. Cai, E. Sedov, S. Klembt, A. V. Kavokin, S. Tongay, K. Watanabe, T. Taniguchi, S. Höfling, and C. Schneider, Bosonic condensation of exciton–polaritons in an atomically thin crystal, Nat. Mater. **20**, 1233 (2021).

[44] R. Su, S. Ghosh, J. Wang, S. Liu, C. Diederichs, T. C. H. Liew, and Q. Xiong, Observation of exciton polariton condensation in a perovskite lattice at room temperature, Nat. Phys. **16**, 301 (2020).

[45] S. Gerhardt, M. Deppisch, S. Betzold, T. H. Harder, T. C. H. Liew, A. Predojević, S. Höfling, and C. Schneider, Polarization-dependent light-matter coupling and highly indistinguishable resonant fluorescence photons from quantum dot-micropillar cavities with elliptical cross section, Phys. Rev. B **100**, 115305 (2019).

[46] K. Kawabata, M. Sato, and K. Shiozaki, Higher-order non-Hermitian skin effect, Phys. Rev. B **102**, 205118 (2020).

[47] D. Leykam, S. Flach, and Y. D. Chong, Flat bands in lattices with non-Hermitian coupling, Phys. Rev. B **96**, 064305 (2017).

[48] X.-W. Luo and C. Zhang, Higher-Order Topological Corner States Induced by Gain and Loss, Phys. Rev. Lett. **123**, 073601 (2019).

[49] T. Liu, Y.-R. Zhang, Q. Ai, Z. Gong, K. Kawabata, M. Ueda, and F. Nori, Second-Order Topological Phases in Non-Hermitian Systems, Phys. Rev. Lett. **122**, 076801 (2019).

[50] R. Okugawa, R. Takahashi, and K. Yokomizo, Second-order topological non-Hermitian skin effects, Phys. Rev. B **102**, 241202(R) (2020).

[51] Y. Song, W. Liu, L. Zheng, Y. Zhang, B. Wang, and P. Lu, Two-dimensional non-Hermitian Skin Effect in a Synthetic Photonic Lattice, Phys. Rev. Appl. **14**, 064076 (2020).

[52] See Supplemental Material at http://link.aps.org/supplemental/10.1103/PhysRevB.106.L201302 for the different loops in Fig. S1(a) that describe the different intergration direction in Sec. S1.

[53] T. Yoshida, T. Mizoguchi, and Y. Hatsugai, Mirror skin effect and its electric circuit simulation, Phys. Rev. Res. **2**, 022062(R) (2020).

[54] K. Yokomizo and S. Murakami, Non-Bloch band theory in bosonic Bogoliubov–de Gennes systems, Phys. Rev. B **103**, 165123 (2021).

[55] X. Xu, H. Xu, S. Mandal, R. Banerjee, S. Ghosh, and T. C. H. Liew, Interaction-induced double-sided skin effect in an exciton-polariton system, Phys. Rev. B **103**, 235306 (2021).

[56] R. Banerjee, S. Mandal, and T. C. H. Liew, Coupling between Exciton-Polariton Corner Modes through Edge States, Phys. Rev. Lett. **124**, 063901 (2020).

[57] H.-R. Kim, M.-S. Hwang, D. Smirnova, K.-Y. Jeong, Y. Kivshar, and H.-G. Park, Multipolar lasing modes from topological corner states, Nat. Commun. **11**, 5758 (2020).

[58] H. Zhong, Y. V. Kartashov, A. Szameit, Y. Li, C. Liu, and Y. Zhang, Theory of topological corner state laser in kagome waveguide arrays, APL Photonics **6**, 040802 (2021).

[59] M. S. Kirsch, Y. Zhang, M. Kremer, L. J. Maczewsky, S. K. Ivanov, Y. V. Kartashov, L. Torner, D. Bauer, A. Szameit, and M. Heinrich, Nonlinear second-order photonic topological insulators, Nat. Phys. **17**, 995 (2021).

[60] See Supplemental Material at http://link.aps.org/supplemental/10.1103/PhysRevB.106.L201302 for the continous model with periodic boundary condition and its energy spectrum that are calculated numerically in Sec. S5.

[61] See Supplemental Material at http://link.aps.org/supplemental/10.1103/PhysRevB.106.L201302 for Sec. S4, which gives a detailed discussion about the non-Hermitian topology with Bogoliubov spetrum.

[62] C.-E. Bardyn, T. Karzig, G. Refael, and T. C. H. Liew, Chiral Bogoliubov excitations in nonlinear bosonic systems, Phys. Rev. B **93**, 020502(R) (2016).

[63] O. Bleu, D. D. Solnyshkov, and G. Malpuech, Interacting quantum fluid in a polariton Chern insulator, Phys. Rev. B **93**, 085438 (2016).

[64] M. Wouters and I. Carusotto, Excitations in a Nonequilibrium Bose-Einstein Condensate of Exciton Polaritons, Phys. Rev. Lett. **99**, 140402 (2007).

[65] M. Wouters, I. Carusotto, and C. Ciuti, Spatial and spectral shape of inhomogeneous nonequilibrium exciton-polariton condensates, Phys. Rev. B **77**, 115340 (2008).

Correction: An incorrect sign and a missing sign in Eq. (1) and an error in the sentence following Eq. (1) have been fixed.